

Optimal Control Theory of the (2+1)-Dimensional BTZ Black Hole

M. Radomirov^{*a}, R. C. Rashkov^{†a,c}, G. S. Stoilov^{‡a}, and T. Vetsov^{§a}

^a*Department of Physics, Sofia University,
5 J. Bourchier Blvd., 1164 Sofia, Bulgaria*

^c*Institute for Theoretical Physics, Vienna University of Technology,
Wiedner Hauptstr. 8–10, 1040 Vienna, Austria*

Abstract

We apply a finite-time geometric optimization framework to investigate thermal fluctuations and (non)equilibrium optimal processes in the $(2 + 1)$ -dimensional BTZ black hole. Employing Hessian thermodynamic information metrics, we construct geodesic trajectories that define optimal protocols connecting distinct thermodynamic configurations. Finite-time state transitions are described by paths that extremize entropy production or energy dissipation, depending on the chosen thermodynamic representation. This work presents the first formulation of a geometric optimal control theory for the BTZ black hole.

Contents

1	Introduction	2
2	Thermodynamics of the BTZ black hole	3
2.1	The BTZ black hole solution	4
2.2	Energy and entropy thermodynamic representations	4
2.3	Thermodynamic stability	5
3	Thermogeometric optimization method (TGO)	5

^{*}Email: radomirov@phys.uni-sofia.bg

[†]Email: rash@phys.uni-sofia.bg

[‡]Email: grigorstoilov234@gmail.com

[§]Email: vetsov@phys.uni-sofia.bg

4	Optimal processes in energy representation	6
4.1	Thermodynamic metric and curvature	6
4.2	Geodesic equations in (S, J) space	7
4.3	Optimal evaporation of the static BTZ black hole	7
4.4	Optimal processes of the rotating BTZ black hole	8
5	Optimal process in entropy representation	13
5.1	Thermodynamic metric and geodesic equations	13
5.2	Optimal evaporation of the static BTZ black hole	13
5.3	Optimal processes of the rotating BTZ black hole	14
6	Conclusion	17
A	Planck parameters in (2+1)-dimensions related to G_3	19
B	The BTZ solution in Planck and other units	19

1 Introduction

A key problem in black hole physics is to characterize the evolution of their thermodynamic states under different physical constraints. Their macroscopic properties can change through processes such as matter accretion [1–5], mergers [6, 7], gravitational-wave emission [8], and Hawking radiation [9]. In addition to their fundamental relevance, these mechanisms have practical implications, such as energy extraction in the Penrose process [10]. This naturally raises the question of whether other mechanisms can also generate changes in black holes’ thermodynamics.

Thermodynamic Geometry (TG) provides the essential tools for addressing this problem [11–13]. By encoding fluctuations in geometric terms, it captures intrinsic relations among macrostates of opened or closed systems. Two widely used constructions are Weinhold’s metric, defined as the Hessian of the internal energy, and Ruppeiner’s metric, defined as the Hessian of the entropy. These are conformally related via the temperature [13–15].

However, the Hessian approach is not always sufficient to capture the full range of physical features in black hole thermodynamics. To address this, Geometrothermodynamics (GTD) was developed [16–19], extending the Hessian framework to construct Legendre-invariant metrics [20]. These geometric methods have since been widely applied to study thermodynamic properties of black holes and other gravitational systems [21–23].

Equipped with appropriate metrics on the space of states, one can introduce geometric structures such as curvature, geodesic paths between states, and thermodynamic length. These quantities play a central role in analyzing fluctuations in (non)equilibrium systems and in formulating valid optimization protocols under certain conditions. Such geometric features are particularly important in the control theory of classical and quantum systems, where the task is to drive the system from one state to another while maximizing efficiency or minimizing losses [24].

In thermodynamic geometry, equilibrium states form a Riemannian manifold whose metric reflects thermal fluctuations [12, 13]. The corresponding scalar curvature has direct physical significance: it is zero for noninteracting systems, negative for attractive interactions, and positive for repulsive ones. Its absolute value relates to the correlation volume and diverges at criticality, mirroring the behavior of statistical correlation lengths. These features make thermodynamic curvature a powerful tool for probing microscopic interactions [21–23].

On the other hand, geodesics on the state space correspond to trajectories that extremize the thermodynamic length [25–27]. They represent the natural notion of shortest paths between points and admit a physical interpretation as statistically preferred fluctuations connecting neighboring states. Within finite-time thermodynamics (FTT) [28–31], geodesics identify minimally

dissipative processes, thus providing a geometric criterion for optimal evolution. Applied to black hole systems [31–35], geodesics have proven effective in characterizing (non)equilibrium dynamics and phase transitions.

Recently, a finite-time geometric optimization framework was introduced to study thermal fluctuations and optimal processes in the state space of Kerr black hole solution [31]. It was shown that geodesic evolution of thermodynamic states can reproduce a Hawking-like evaporation of the Kerr black hole, albeit arising from entirely different physical mechanisms. These optimal evaporation processes manifest as fluctuations on the event horizon, which may occur spontaneously or be triggered by external accretion. The thermodynamic length determines both the likelihood of such optimal processes and the duration over which they proceed.

The aim of this work is to investigate thermal fluctuations and optimal processes on the event horizon of the Bañados–Teitelboim–Zanelli (BTZ) black hole within the finite-time geometric optimization framework developed in [31]. The BTZ solution describes a black hole in $(2 + 1)$ -dimensional Anti-de Sitter spacetime (AdS_3) [36]. First identified in 1992, it serves as a lower-dimensional analogue of more familiar $(3 + 1)$ -dimensional black holes such as the Schwarzschild and Kerr solutions. Owing to its reduced dimensionality, the BTZ black hole is mathematically more tractable and thus widely employed as a simplified model in theoretical investigations. Moreover, its asymptotically AdS geometry, rather than flat spacetime, renders it particularly important in the context of the AdS/CFT correspondence and holography¹.

The paper is structured as follows. In Section 2 we summarize the fundamental thermodynamic properties of the BTZ black hole, expressed in both SI and $3d$ Planck units. In Section 3, we briefly review the key aspects of the Thermogeometric Optimization (TGO) method introduced in [31]. In Section 4, we analyze thermal fluctuations and optimal processes in the energy representation for both static and rotating BTZ black holes. We show that the system consistently evolves toward a static (non-rotating) configuration with well-defined energy and entropy. In Section 5 we consider the entropy representation, where several qualitatively distinct final configurations were identified. In particular, some optimal trajectories asymptotically drive the system toward near-extremal BTZ states – although this limit remains unattainable within finite time in accordance with the third law of thermodynamics. Other trajectories drive the black hole toward a fixed, nonzero specific spin, while some processes inevitably lead to static configurations within finite time. Finally, Section 6 presents a brief discussion of our findings.

2 Thermodynamics of the BTZ black hole

We shortly review the fundamental thermodynamic relations for the BTZ black hole in both the energy and entropy ensembles, with all quantities expressed in SI units. The conversion to Planck and other units is detailed in Appendix A.

¹The BTZ solution is holographically dual to a thermal state in a two-dimensional conformal field theory (CFT_2) living on the asymptotic boundary of AdS_3 [37]. The black hole mass and angular momentum are directly related to the energy and momentum of the dual CFT, while the Hawking temperature and entropy are reproduced by the thermal properties of the boundary theory [38]. In particular, the microscopic entropy of the BTZ black hole can be derived from the Cardy formula for the asymptotic density of states in a unitary two-dimensional CFT with central charge² $\tilde{c} = 3\ell/(2G_3)$, obtained from the Brown-Henneaux analysis of the AdS_3 asymptotic symmetry algebra [39]. This remarkable agreement established one of the earliest and most explicit demonstrations of holography in lower dimensions, and it continues to serve as a foundational example in the study of black hole thermodynamics and quantum aspects of gravity.

2.1 The BTZ black hole solution

The BTZ black hole metric in $D = 2 + 1$ dimensions is given by [36, 40]:

$$ds^2 = -\frac{(r^2 - r_+^2)(r^2 - r_-^2)}{\ell^2 r^2} c^2 dt^2 + \frac{\ell^2 r^2}{(r^2 - r_+^2)(r^2 - r_-^2)} dr^2 + r^2 \left(d\varphi - \frac{r_+ r_-}{\ell r^2} c dt \right)^2, \quad (2.1)$$

where c is the speed of light, ℓ is the AdS radius, r_+ is the event horizon, and r_- is the inner Cauchy horizon. The energy³ E , angular momentum J , entropy S , Hawking temperature T , and angular velocity Ω of the BTZ black hole solution are given by⁴:

$$S = \frac{\pi k c^3}{2 \hbar G_3} r_+, \quad E = \frac{r_+^2 + r_-^2}{8 G_3 \ell^2} c^4, \quad J = \frac{c^3}{4 G_3 \ell} r_+ r_-, \quad T = \frac{\hbar c}{k} \frac{r_+^2 - r_-^2}{2 \pi \ell^2 r_+}, \quad \Omega = c \frac{r_-}{\ell r_+}, \quad (2.2)$$

These determine the thermodynamics of the BTZ system with first law and a Smarr relation:

$$dE = T dS + \Omega dJ, \quad E = \frac{1}{2} T S + \Omega J. \quad (2.3)$$

2.2 Energy and entropy thermodynamic representations

Solving Eqs. (2.2) for r_{\pm} in terms of the relevant thermodynamic parameters one can find the fundamental relations for energy and entropy:

$$E(S, J) = \frac{\zeta^2 S^4 + \lambda^2 J^2}{2 \lambda S^2}, \quad S(E, J) = \frac{1}{\zeta} \sqrt{\lambda(E + \sqrt{E^2 - \zeta^2 J^2})}, \quad (2.4)$$

where following notations were introduce:

$$\lambda = \frac{\pi^2 c^4 k^2}{G_3 \hbar^2}, \quad \zeta = \frac{c}{\ell}. \quad (2.5)$$

The temperature and the angular velocity follow naturally in energy representation:

$$T = \left. \frac{\partial E}{\partial S} \right|_J = \frac{\zeta^2 S^4 - \lambda^2 J^2}{\lambda S^3}, \quad \Omega = \left. \frac{\partial E}{\partial J} \right|_S = \frac{J \lambda}{S^2}. \quad (2.6)$$

In entropy representation one has:

$$T = \left(\frac{\partial S}{\partial E} \right)_J^{-1} = \frac{2 \zeta \sqrt{E^2 - \zeta^2 J^2}}{\sqrt{\lambda(E + \sqrt{E^2 - \zeta^2 J^2})}}, \quad \Omega = -T \left. \frac{\partial S}{\partial J} \right|_E = \frac{\zeta^2 J}{E + \sqrt{E^2 - \zeta^2 J^2}}. \quad (2.7)$$

Non-extremality requires the temperature of the BTZ black hole always be positive ($T > 0$), which in the corresponding representations leads to⁵:

$$\zeta J < E \quad \text{or} \quad \lambda J < \zeta S^2. \quad (2.8)$$

Note that the extremal case $\zeta J = E$ is omitted since it violates classically the third law of thermodynamics. One can write (2.8) in terms of the BTZ dimensionless specific spin⁶ $a \in [0, 1)$:

$$a = \frac{\zeta J}{E}, \quad 0 \leq a < 1. \quad (2.9)$$

The non-extremality condition $a < 1$ imposes a constraint on the boundary quantum dynamics via the dimensionless central charge \tilde{c} of the dual conformal field theory (CFT), i.e. [41]:

$$\tilde{c} = \frac{3 c^3 \ell}{2 G_3 \hbar} < \frac{3 \hbar}{2 \pi^2 k^2} \frac{S^2}{J}, \quad (2.10)$$

thereby setting an upper bound on the effective number of degrees of freedom in the dual CFT.

³The standard relation between mass and energy $E = M c^2$ is assumed.

⁴Here \hbar is the Dirac constant, k is the Boltzmann constant, and G_3 is the 3-dimensional gravitational constant with units: $\text{m}^2 \cdot \text{kg}^{-1} \cdot \text{s}^{-2}$.

⁵The case $T = 0$ ($r_+ = r_-$) violates classically the third law of thermodynamics.

⁶Note that, assuming $G_3 > 0$, Eq. (2.2) imposes $J \geq 0$, thus $0 \leq a < 1$.

2.3 Thermodynamic stability

The BTZ black hole is globally stable from classical thermodynamic point of view. This follows either from the eigenvalue criterion or the Sylvester criterion for positive-definiteness of the Hessian of the energy (energy is strictly convex) [42, 43]:

$$\left. \frac{\partial^2 E}{\partial S^2} \right|_J = \frac{\zeta^2 S^4 + 3\lambda^2 J^2}{\lambda S^4} > 0, \quad \left. \frac{\partial^2 E}{\partial J^2} \right|_S = \frac{\lambda}{S^2} > 0, \quad \det \hat{H} = \frac{\zeta^2 S^4 - \lambda^2 J^2}{S^6} > 0. \quad (2.11)$$

The first two inequalities reflect the convexity of energy along its natural parameters, and the third one assures full convexity according to the Sylvester criterion.

Since the non-extremal BTZ solution is globally stable, it should also be locally stable, e.g. all heat capacities must be strictly positive [42]:

$$C_E(S, J) = T \left. \frac{\partial S}{\partial T} \right|_E = T \frac{\{S, E\}_{S, J}}{\{T, E\}_{S, J}} = \frac{S(\zeta^2 S^4 - \lambda^2 J^2)}{3\zeta^2 S^4 + \lambda^2 J^2} > 0, \quad (2.12)$$

$$C_J(S, J) = T \left. \frac{\partial S}{\partial T} \right|_J = T \frac{\{S, J\}_{S, J}}{\{T, J\}_{S, J}} = \frac{S(\zeta^2 S^4 - \lambda^2 J^2)}{\zeta^2 S^4 + 3\lambda^2 J^2} > 0, \quad (2.13)$$

$$C_\Omega(S, J) = T \left. \frac{\partial S}{\partial T} \right|_\Omega = T \frac{\{S, \Omega\}_{S, J}}{\{T, \Omega\}_{S, J}} = S > 0. \quad (2.14)$$

Here we used Nambu brackets (see [42]) to find the corresponding heat capacities. The result shows that there are no Davies phase transition curves for BTZ, besides the extremal one (2.8).

The global stability of the BTZ black hole implies that it cannot evaporate solely through standard Hawking radiation. However, like all physical systems, black holes are susceptible to spontaneous thermal or quantum fluctuations, as well as external perturbations at their event horizons. Such effects can induce changes in the black hole's parameters, potentially driving an evaporation-like evolution that decreases its mass-energy content.

In the following sections, we apply the thermogeometric optimization method to the BTZ system to investigate this behavior. The TGO method is specifically designed to study optimal processes in thermal systems, including black holes [31].

3 Thermogeometric optimization method (TGO)

The Thermogeometric Optimization (TGO) method, introduced in [31], provides a systematic framework for analyzing thermal fluctuations and optimal processes on black hole event horizons. The procedure begins by specifying a natural thermodynamic potential Φ , determined by the system's control parameters, together with its associated thermodynamic metric \hat{g} . Within thermodynamic geometry, two metric formulations are commonly employed, namely Weinhold's metric, defined as the Hessian of the energy⁷ ($\Phi \equiv E$) [11]:

$$ds_W^2 = \epsilon \sum_{a,b=1}^n \frac{\partial^2 E}{\partial E^a \partial E^b} dE^a dE^b, \quad \epsilon \in \mathbb{R}, \quad (3.1)$$

and Ruppeiner's metric⁸, defined as the Hessian of the entropy⁹ ($\Phi \equiv S$) [12, 13]:

$$ds_R^2 = \epsilon \sum_{a,b=1}^n \frac{\partial^2 S}{\partial S^a \partial S^b} dS^a dS^b. \quad (3.2)$$

⁷In its original form, Weinhold's metric is defined with $\epsilon = +1$.

⁸Importantly, these two metrics are conformally related through the temperature [13–15].

⁹In its original form, Ruppeiner's metric is defined with $\epsilon = -1$.

Here, E^a denote the natural control variables of the energy E , while S^a are those associated to the entropy S . The parameter ϵ , introduced in [31], extends the equilibrium setup of TG to include also non-equilibrium situations.

The next step is to parametrize the natural coordinates Φ^a of the potential Φ with an affine time parameter t and extremize the thermodynamic length in order to obtain the thermodynamic geodesics with respect to the chosen metric. The later can be interpreted as fluctuation paths or optimal protocols. By definition the thermodynamic length functional is given by:

$$\mathcal{L}[\gamma(t)] = \int_0^\tau \sqrt{g_{ab}(\vec{\Phi}(t)) \dot{\Phi}^a(t) \dot{\Phi}^b(t)} dt, \quad (3.3)$$

and the corresponding system of geodesic equations yield:

$$\ddot{\Phi}^c(t) + \Gamma_{ab}^c(\hat{g}, \vec{\Phi}) \dot{\Phi}^a(t) \dot{\Phi}^b(t) = 0, \quad (3.4)$$

where $\Gamma_{ab}^c(\hat{g}, \vec{\Phi})$ are the standard Christoffel symbols, defined by:

$$\Gamma_{ab}^c = \frac{1}{2} g^{cd} (\partial_a g_{db} + \partial_b g_{da} - \partial_d g_{ab}). \quad (3.5)$$

4 Optimal processes in energy representation

We employ the TGO framework to study the finite-time evolution of optimal processes on the event horizon of the BTZ black hole, formulated in the energy representation. Within this approach, we demonstrate how the BTZ system can either lose or gain energy through a “least resistant” paths on the space of its macrostates.

4.1 Thermodynamic metric and curvature

The natural thermodynamic metric in energy representation is the Weinhold metric:

$$ds^2 = \epsilon \frac{\zeta^2 S^4 + 3\lambda^2 J^2}{\lambda S^4} dS^2 - \epsilon \frac{\lambda J}{S^3} dS dJ + \epsilon \frac{\lambda}{S^2} dJ^2. \quad (4.1)$$

Its thermodynamic curvature is given by:

$$R = \frac{2\lambda\zeta^2 S^6}{\epsilon(\zeta S^2 - \lambda J)^2(\zeta S^2 + \lambda J)^2}. \quad (4.2)$$

It is divergent along the extremal curve $\zeta S^2 = J\lambda$, where interactions become infinitely strong. The nature of the underlying information geometry is governed by the sign of the scaling parameter ϵ . For $\epsilon > 0$, the information space is elliptic with positive curvature $R > 0$, whereas for $\epsilon < 0$, a hyperbolic information geometry with $R < 0$ emerges.

The Weinhold thermodynamic curvature R is shown in Fig. 1 as a function of S and J . Since R quantifies the effective interaction strength among horizon degrees of freedom, it is observed that the interactions intensify in the vicinity of the extremal BTZ curve (dashed red), where a phase transition occurs. As we show in Section 4.3 in energy representation $\epsilon > 0$ ensures a positive-definite thermodynamic length, thus the curvature R remains positive, implying that the information geometry is intrinsically elliptic.

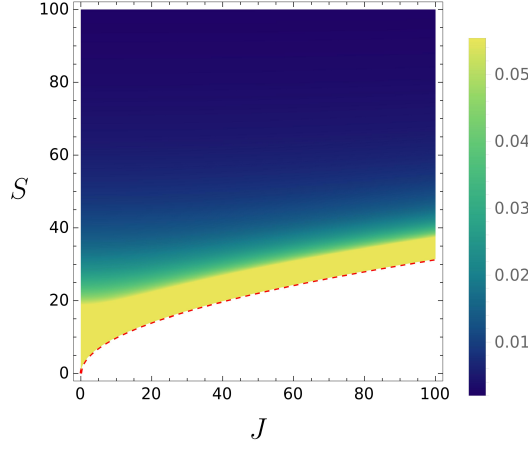


Figure 1: The Weinhold thermodynamic curvature R is presented as a function of S and J in Planck units with $\ell = 1$. An increase in the interaction strength among the horizon degrees of freedom is observed near the extremal BTZ curve (dashed red), where a phase transition takes place. In the asymptotic regime, far from extremality, the thermodynamic geometry of the BTZ black hole approaches flatness, indicating weak or negligible interactions. Since $\epsilon > 0$ ensures a positive-definite thermodynamic length, the curvature R remains positive, implying that the information geometry is elliptic.

4.2 Geodesic equations in (S, J) space

We parametrize the (S, J) coordinates by an affine time parameter t and seek to obtain their optimal profiles by solving the geodesic equations on the space of macrostates in energy ensemble:

$$\ddot{S} + \Gamma_{SS}^S(S, J)\dot{S}^2 + 2\Gamma_{SJ}^S(S, J)\dot{S}\dot{J} + \Gamma_{JJ}^S(S, J)\dot{J}^2 = 0, \quad (4.3)$$

$$\ddot{J} + \Gamma_{JJ}^J(S, J)\dot{J}^2 + 2\Gamma_{SJ}^J(S, J)\dot{S}\dot{J} + \Gamma_{SS}^J(S, J)\dot{S}^2 = 0, \quad (4.4)$$

where the Christoffel symbols are given by:

$$\Gamma_{SS}^S = 0, \quad \Gamma_{SJ}^S = \frac{J\lambda^2}{\zeta^2 S^4 - J^2 \lambda^2}, \quad \Gamma_{JJ}^S = \frac{\lambda^2 S}{J^2 \lambda^2 - \zeta^2 S^4}, \quad (4.5)$$

$$\Gamma_{SS}^J = \frac{3J}{S^2}, \quad \Gamma_{SJ}^J = \frac{3J^2 \lambda^2 - \zeta^2 S^4}{\zeta^2 S^5 - J^2 \lambda^2 S}, \quad \Gamma_{JJ}^J = \frac{2J \lambda^2}{J^2 \lambda^2 - \zeta^2 S^4}. \quad (4.6)$$

The solutions to these nonlinear equations define the optimal profiles for entropy $S(t)$ and angular momentum $J(t)$ at various initial conditions:

$$S(0) = S_0, \quad \dot{S}(0) = \dot{S}_0, \quad J(0) = J_0, \quad \dot{J}(0) = \dot{J}_0, \quad (4.7)$$

where S_0 and J_0 denote the initial entropy and angular momentum of the BTZ black hole, respectively, and \dot{S}_0 and \dot{J}_0 represent their initial rates of change. It is important to note that $S(t)$ and $J(t)$ represent valid geodesic profiles only when the thermodynamic length \mathcal{L} along the path is real and positive. The profiles for energy $E(t)$ and specific spin $a(t)$ follow from their definitions (2.4) and (2.9).

4.3 Optimal evaporation of the static BTZ black hole

A simple analytical solution exists for the static ($J = 0$) BTZ black hole. In this case, the second equation (4.4) is trivially satisfied, while the first equation (4.3) becomes $\ddot{S}(t) = 0$ leading to a

simple linear profile of the entropy¹⁰:

$$S(t) = S_0 - |\dot{S}_0|t. \quad (4.8)$$

Here we already assumed an evaporation process with an initial rate: $\dot{S}_0 = -|\dot{S}_0| < 0$. The thermodynamic length of the process from S_0 to S_τ at $t = \tau$ is given by:

$$\mathcal{L}_{S_0 \rightarrow S_\tau} = \int_0^\tau \sqrt{g_{ab} \dot{x}^a(t) \dot{x}^b(t)} dt = \zeta \sqrt{\frac{\epsilon}{\lambda}} |\dot{S}_0| \tau = v\tau, \quad (4.9)$$

where $x^a(t) = (S(t), J(t) = 0)$, and v is the thermodynamic speed of the process. The length is real and positive if $\epsilon > 0$, hence it defines an elliptic information space ($R > 0$). Additionally, in the static case we have only entropy, thus one can also find the direct thermodynamic length¹¹:

$$\mathcal{L}_{S_0 \rightarrow S_\tau} = \int \sqrt{g_{ab} dx^a dx^b} = -\zeta \sqrt{\frac{\epsilon}{\lambda}} \int_{S_0}^{S_\tau} dS = \zeta \sqrt{\frac{\epsilon}{\lambda}} (S_0 - S_\tau), \quad (4.10)$$

where $x^a = (S, J = 0)$. Insisting on both lengths be equal, we can make an estimation of the average relaxation time $\bar{\tau}$ of the process:

$$\bar{\tau} \approx \frac{S_0 - S_\tau}{|\dot{S}_0|}. \quad (4.11)$$

Since $S_0 > S_\tau$ in the evaporation process, the parameter $\bar{\tau} > 0$. This indicates that the average relaxation time is proportional to the entropy change $\Delta S = S_0 - S_\tau$ produced by the BTZ black hole during the process. In the case of complete evaporation ($S_\tau = 0$), the total evaporation time can be obtained from the condition $S(t_{\text{evap}}) = 0$, yielding:

$$t_{\text{evap}} = \frac{S_0}{|\dot{S}_0|}. \quad (4.12)$$

Hence, the evaporation thermodynamic length:

$$\mathcal{L}_{\text{evap}} = \zeta \sqrt{\frac{\epsilon}{\lambda}} S_0 = \frac{\hbar \sqrt{\epsilon G_3}}{\pi c k \ell} S_0. \quad (4.13)$$

Since the evaporation length is proportional solely to the initial entropy S_0 of the BTZ black hole, this indicates that larger black holes are less likely to undergo spontaneous evaporation. Conversely, smaller black holes may evaporate spontaneously with higher probability.

The quantity \mathcal{L}^2 has units of energy, which aligns with its interpretation as the minimal energy required to drive the system from one thermodynamic state to another. The latter can be used to determine the scale factor ϵ for a complete evaporation process of the BTZ. Insisting on \mathcal{L}^2 be at least the initial energy of the BTZ black hole $E_0 = \zeta^2 S_0^2 / (2\lambda)$, then we find $\epsilon = 1/2$.

4.4 Optimal processes of the rotating BTZ black hole

We examine how optimal processes, initiated at different initial rates of the parameters, can transform the thermodynamic state of a rotating BTZ black hole. In all cases considered – within the energy representation – the system evolves toward a static (non-rotating) black hole

¹⁰It is important to note that the optimal evaporation process follows paths of “least resistance” and, as such, is not constrained to obey the Stefan–Boltzmann or similar blackbody power laws in (2+1)-dimensions. Consequently, Hawking evaporation and optimal evaporation models may exhibit significant differences. For further discussion, see [31].

¹¹Note that $\sqrt{g_{ab} \dot{x}^a \dot{x}^b} \propto \sqrt{dS^2} = |dS| = -dS > 0$, since entropy decreases during an evaporation process.

with well-defined energy and entropy, and thus no complete evaporation of the rotating BTZ black hole occurs. However, the final energy and entropy may either increase or decrease, depending on the initial rates. We refer to processes that reduce both energy and entropy as optimal evaporation of the BTZ black hole. Conversely, when the final state exhibits higher energy and entropy, we have accretion-type process¹² (traditionally called).

4.4.1 Setting up initial conditions

We will numerically integrate the geodesic equations (4.3) and (4.4) in energy representation. For consistency of numerical results, all quantities are rendered dimensionless and expressed in Planck units (see Appendix A). The resulting solutions represent valid geodesic trajectories – interpreted as optimal thermodynamic processes in the (S, J) parameter space – provided that the thermodynamic length, defined by the integral (3.3), remains real and positive-definite.

It is important to note that the algorithm does not encode or refer to any specific physical mechanism underlying the process. As a result, each geodesic represents a distinct optimal process, and multiple geodesics originating from the same initial state may intersect at a later point in the state space. That is, there may exist multiple optimal ways to transition between the same two thermodynamic states¹³.

The initial state will be defined by the following initial parameters of the BTZ black hole:

$$S_0 = 5, \quad J_0 = 1, \quad E_0 = \frac{\pi^2 J_0^2}{2S_0^2} + \frac{S_0^2}{2\pi^2 \ell^2} = 1.46, \quad a_0 = \frac{J_0}{E_0 \ell} = 0.68, \quad (4.14)$$

where we set $\ell = 1$. It is convenient to represent the initial rates of change of the parameters at $t = 0$ in polar coordinates (u, ϕ) by:

$$\dot{S}_0 = u \sin \phi, \quad \dot{J}_0 = u \cos \phi, \quad u = \sqrt{\dot{S}_0^2 + \dot{J}_0^2}, \quad \tan \phi = \frac{\dot{S}_0}{\dot{J}_0}, \quad (4.15)$$

where the angle ϕ determines the initial direction of the geodesic trajectory of states in (S, J) space. The corresponding initial rates of energy \dot{E}_0 and specific spin a_0 are then determined by evaluating the time derivatives of their numerical profiles at $t = 0$. Comparable results for other angles ϕ are summarized in Table 1.

We can characterize the evolution of a given parameter X by its relative change δX (in %):

$$\delta X = \frac{X(\tau) - X(0)}{X(0)} \times 100\%, \quad (4.16)$$

where τ typically denotes the duration of the process (the relaxation time). The relative change δX is positive if X increases over time and negative if it decreases.

In the following subsections, we illustrate the TGO method by fixing $u = 0.01$ and examining in detail two representative cases: $\phi = 0^\circ$ (accretion-driven) and $\phi = 240^\circ$ (optimal evaporation process). The corresponding geodesic trajectories in the (S, J) space for a wider range of initial angles, $\phi = \{0^\circ, 45^\circ, 60^\circ, 90^\circ, 135^\circ, 180^\circ, 225^\circ, 240^\circ, 270^\circ, 315^\circ\}$, along with the associated thermodynamic curvature, are displayed in Fig. 4.

¹²An internal reconfiguration of the black hole states, driven by thermal or quantum fluctuations, may also lead to an increase in both energy and entropy at the expense of angular momentum. In such cases, no external driving (accretion) force is required to initiate or sustain the process.

¹³Multiple optimal processes may correspond to different physical mechanisms – such as conduction versus radiation – or may arise under differing external constraints. A classic example of intersecting geodesics is provided by distinct great circles on a sphere, which always intersect at two antipodal points. Since, in our case, (S, J) space exhibits positive curvature, similar to a sphere, the existence of intersecting geodesics is allowed.

4.4.2 Optimal process at $\phi = 0^\circ$

In this case, the final configuration is a static ($a_\tau = 0$) BTZ black hole with $E_\tau = 103 E_0$ and $S_\tau = 11 S_0$. It is characterized by a significant increase in energy and entropy, $\delta E = +10226\%$ and $\delta S = +992\%$, as shown on Figs. 2a and 2b. Note that the profiles on Fig. 2b, with respect to a , are multi-valued functions, since the specific spin $a(t)$ has a local maximum (Fig. 2c).

The results indicate that the optimal process is driven by accretion, whereby matter or energy is supplied to the system. This leads to an initial increase in the black hole's energy, entropy, and angular momentum, with the specific spin peaking at $a_{\text{peak}} \approx 0.994$ (Fig. 2c). Beyond this peak, $a(t)$ gradually decreases – naturally avoiding any violation of the third law – and ultimately vanishes in the final state. This final configuration corresponds to the endpoint of the associated geodesic trajectory in the (S, J) space (Fig. 2d). The subsequent evolution of the BTZ system can then be understood by analyzing the static case discussed in Sec. 4.3.

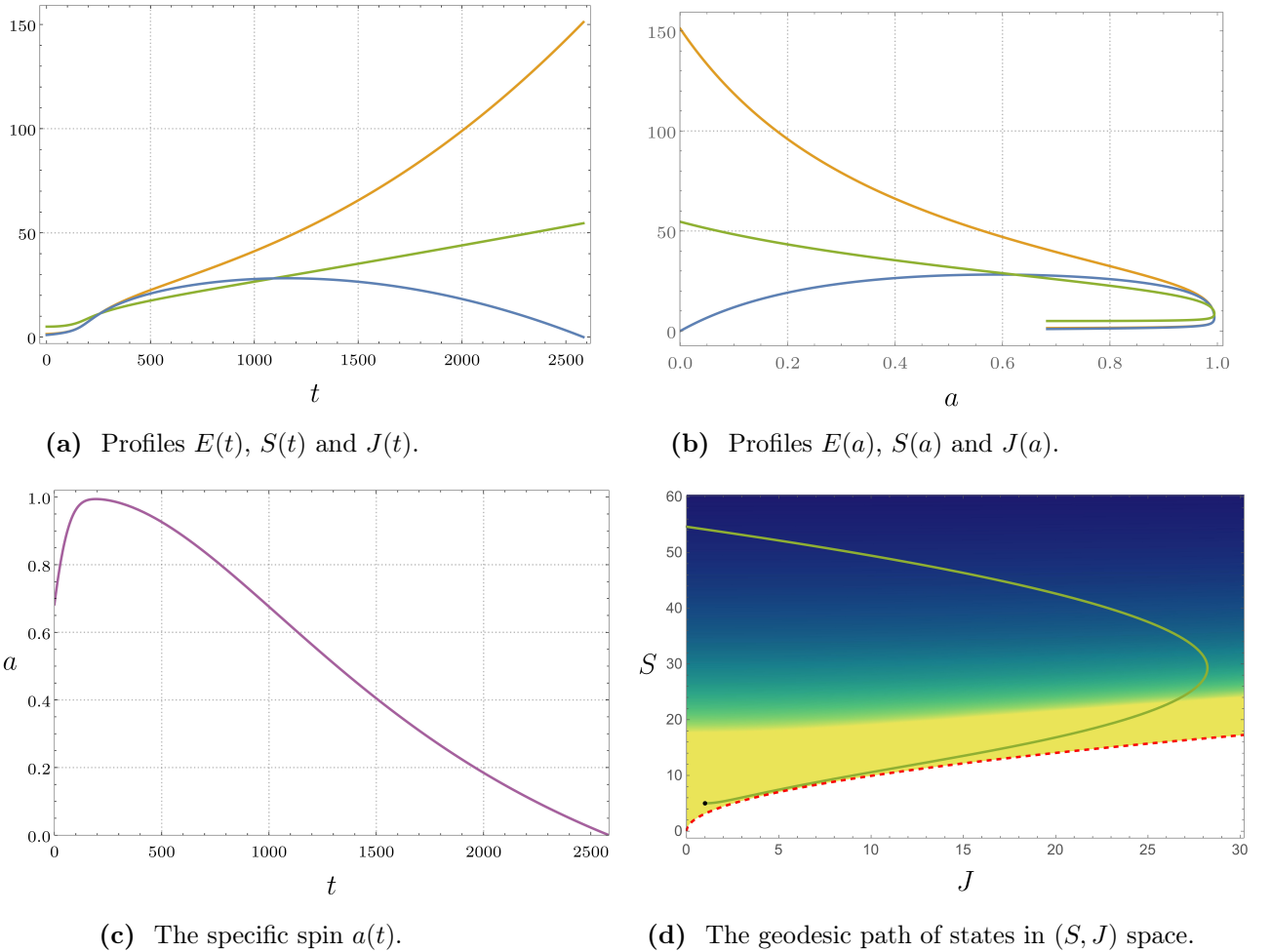


Figure 2: Profiles for $\phi = 0^\circ$. (a) Time evolution of E (orange), S (green), and J (blue). (b) The dependence of E , S , and J on the specific spin a . The final configuration corresponds to a static BTZ black hole with $E_\tau = 151$ and $S_\tau = 55$ in Planck units. (c) Time evolution of the specific spin $a(t)$. It peaks at $a_{\text{peak}} \approx 0.994$ indicating the state closest to extremality, and then gradually decreases to zero. (d) The geodesic trajectory of states (green curve) in (S, J) space, with a starting point at $S_0 = 5$ and $J_0 = 1$ (the black dot), terminates when the angular momentum vanishes. The extremal states are depicted by the dashed red curve.

4.4.3 Optimal process at $\phi = 240^\circ$

At $\phi = 240^\circ$ the final state is a static BTZ black hole with reduced parameters: $E_\tau = 0.3 E_0$ and $S_\tau = 0.6 S_0$, corresponding to a decrease in energy $\delta E = -71\%$ and entropy $\delta S = -42\%$. Such an optimal evaporation may only occur through some physical emission of radiation (scalar, vector, or gravitational modes).

Table 1 demonstrates that as the initial angle ϕ increases from 240° , the extent of evaporation also grows, peaking around $\phi = 259^\circ$, where the system approaches its closest point to complete evaporation. Beyond this angle, the evaporation effect weakens, and accretion-driven processes begin to dominate the evolution. It is important to note, however, that complete direct evaporation of the rotating BTZ is never achieved within the energy representation.

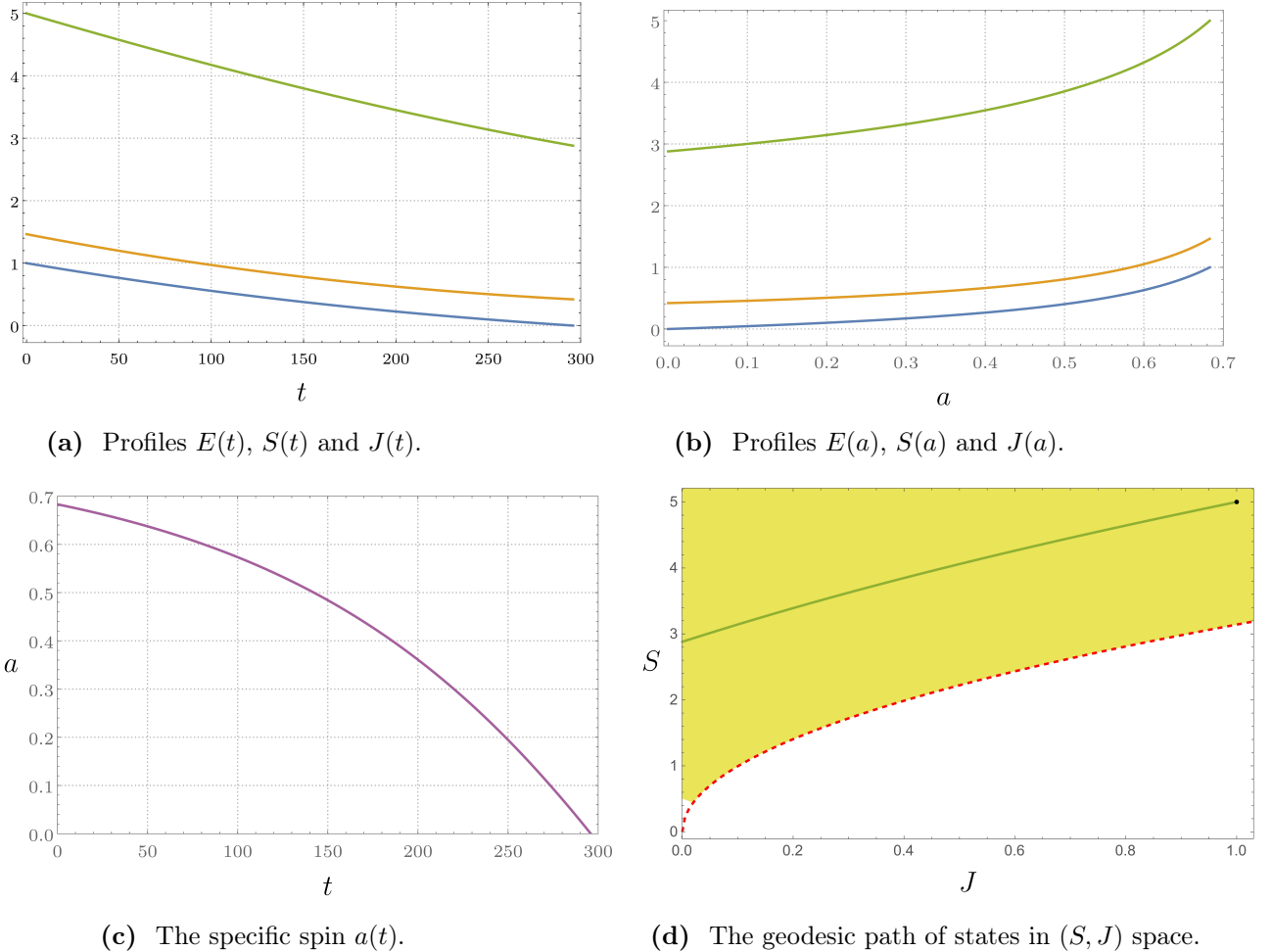


Figure 3: Profiles for $\phi = 240^\circ$. (a) Time evolution of E (orange), S (green), and J (blue). (b) The dependence of E , S , and J on the specific spin a . The final configuration corresponds to a static BTZ black hole with $E_\tau = 0.4$ and $S_\tau = 2.9$ in Planck units. (c) The evolution of $a(t)$ is strictly monotonic, tending towards zero. (d) The geodesic trajectory of states (green curve) in (S, J) space, with a starting point $S_0 = 5$ and $J_0 = 1$ (black dot), terminates when the angular momentum vanishes. Extremality is depicted by the dashed red curve.

4.4.4 Summary for additional process

Figure 4 illustrates several geodesic trajectories in the (S, J) space, with the corresponding data¹⁴ summarized in Table 1. The results show that for initial angles ϕ between 0° and 180° ,

¹⁴The data in the table is rounded up to two relevant digits.

the dynamics is dominated by accretion-driven optimal processes. As ϕ increases beyond 180° , evaporation processes become increasingly significant, reaching a maximum around $\phi = 259^\circ$, where the system comes closest to complete evaporation. Beyond this point, the influence of evaporation diminishes, and accretion-driven behavior once again dominates.

Notably, full evaporation of the rotating BTZ black hole is never realized within the energy representation. The final configuration always corresponds to a static state ($a_\tau = 0$) with non-zero energy and entropy.

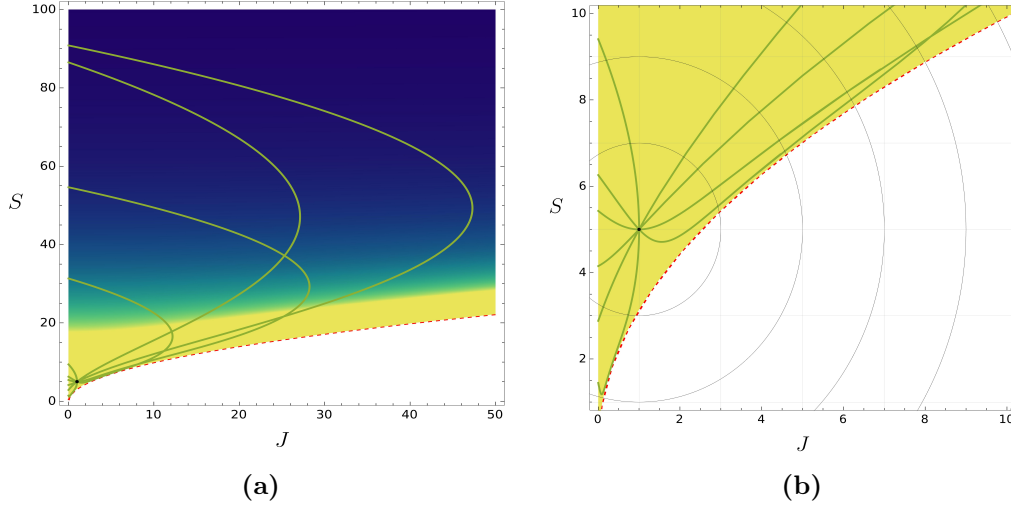


Figure 4: Geodesics paths of states in (S, J) space. **(a)** The thermodynamic curvature R is represented as a colored background. The initial state ($S_0 = 5, J_0 = 1$) lies in a relatively strong curved region (yellow) with high interactions, though it remains sufficiently distant from the extremal boundary (the dashed red curve). **(b)** A magnified view near the initial point. Polar circles help visualize the initial angles ϕ , which determine the direction of each geodesic. All paths naturally avoid extremality and drive the system to a static BTZ black hole configuration.

ϕ	$\dot{E}_0 10^{-3}$	$\dot{S}_0 10^{-3}$	$\dot{J}_0 10^{-3}$	$\dot{a}_0 10^{-3}$	a_τ	E_τ	$\delta E \%$	S_τ	$\delta S \%$	τ	\mathcal{L}^2
0°	3.9	0.0	10	5.0	0.0	151	$+10^4$	55	$+10^3$	2584	264
45°	5.8	7.1	7.1	2.1	0.0	418	$+10^4$	91	$+10^3$	8070	741
60°	5.7	8.7	5.0	0.8	0.0	379	$+10^4$	87	$+10^3$	9539	668
90°	4.3	10	0.0	-2.0	0.0	4.5	+200	9.4	+88	421	2.6
135°	0.2	7.1	-7.1	-4.9	0.0	2.0	+33	6.3	+25	122	0.6
180°	-3.9	0.0	-10	-5.0	0.0	1.5	+0	5.4	+9	106	0.5
225°	-5.8	-7.1	-7.1	-2.1	0.0	0.9	-40	4.1	-17	185	0.4
240°	-5.7	-8.7	-5.0	-0.8	0.0	0.4	-73	2.9	-42	296	0.6
259°	-4.9	-9.8	-1.9	1.0	0.0	0.02	-99	0.7	-86	408	1.6
270°	-4.3	-10	0.0	2.0	0.0	0.1	-93	1.4	-72	354	1.9
315°	-0.2	-7.1	7.1	4.9	0.0	50	$+10^3$	31	+527	1439	89

Table 1: The table summarizes the initial rates of key parameters across various processes. It also indicates how the final state differs from the initial BTZ configuration after each process. Additionally, the duration τ of the process (in Planck units) and the thermodynamic length squared, \mathcal{L}^2 , are provided. The thermodynamic length \mathcal{L}^2 quantifies the minimal energy required to perform the transformation. Smaller \mathcal{L} indicates higher probability for the process to occur.

5 Optimal process in entropy representation

We now proceed by investigating optimal processes on the space of macrostates of the BTZ black hole in entropy representation.

5.1 Thermodynamic metric and geodesic equations

The Ruppeiner metric is given by the Hessian of entropy (2.4) in (E, J) space:

$$\hat{g} = \epsilon \begin{pmatrix} \frac{\partial^2 S}{\partial E^2} \Big|_J & \frac{\partial^2 S}{\partial E \partial J} \\ \frac{\partial^2 S}{\partial E \partial J} & \frac{\partial^2 S}{\partial J^2} \Big|_E \end{pmatrix} = \epsilon \begin{pmatrix} \frac{(U-2E)\sqrt{\lambda(E+U)}}{4\zeta(E-\zeta J)^{3/2}(E+\zeta J)^{3/2}} & -\frac{\zeta J \sqrt{\lambda}(\zeta^2 J^2 - 3E(E+U))}{4(E+U)^{3/2}(E-\zeta J)^{3/2}(E+\zeta J)^{3/2}} \\ -\frac{\zeta J \sqrt{\lambda}(\zeta^2 J^2 - 3E(E+U))}{4(E+U)^{3/2}(E-\zeta J)^{3/2}(E+\zeta J)^{3/2}} & \frac{\zeta(U-2E)\sqrt{\lambda(E+U)}}{4(E-\zeta J)^{3/2}(E+\zeta J)^{3/2}} \end{pmatrix}, \quad (5.1)$$

where $U = \sqrt{E^2 - \zeta^2 J^2}$. Its thermodynamic curvature is zero, thus realizing a flat information space. We parametrize the (E, J) coordinates by an affine time parameter t and seek to obtain their optimal profiles by solving the geodesic equations on the space of macrostates:

$$\ddot{E} + \Gamma_{EE}^E \dot{E}^2 + 2\Gamma_{EJ}^E \dot{E} \dot{J} + \Gamma_{JJ}^E \dot{J}^2 = 0, \quad (5.2)$$

$$\ddot{J} + \Gamma_{JJ}^J \dot{J}^2 + 2\Gamma_{EJ}^J \dot{E} \dot{J} + \Gamma_{EE}^J \dot{E}^2 = 0. \quad (5.3)$$

The corresponding Christoffel symbols are given by:

$$\Gamma_{EE}^E = \frac{3E}{4\zeta^2 J^2 - 4E^2}, \quad \Gamma_{EJ}^E = \frac{3\zeta^2 J}{4E^2 - 4\zeta^2 J^2}, \quad \Gamma_{JJ}^E = \frac{3E\zeta^2}{4\zeta^2 J^2 - 4E^2}, \quad (5.4)$$

$$\Gamma_{EE}^J = \frac{3J}{4E^2 - 4\zeta^2 J^2}, \quad \Gamma_{EJ}^J = \frac{3E}{4\zeta^2 J^2 - 4E^2}, \quad \Gamma_{JJ}^J = \frac{3\zeta^2 J}{4E^2 - 4\zeta^2 J^2}. \quad (5.5)$$

The solutions to these nonlinear equations define the optimal paths for energy $E(t)$ and angular momentum $J(t)$ at various initial conditions:

$$E(0) = E_0, \quad \dot{E}(0) = \dot{E}_0, \quad J(0) = J_0, \quad \dot{J}(0) = \dot{J}_0, \quad (5.6)$$

where E_0 and J_0 denote the initial energy and angular momentum of the BTZ black hole, respectively, and \dot{E}_0 and \dot{J}_0 represent their initial rates of change.

5.2 Optimal evaporation of the static BTZ black hole

In the static case ($J = 0$) we can find explicit solution to the energy profile:

$$E(t) = E_0 \left(1 - \frac{|\dot{E}_0|}{4E_0} t \right)^4. \quad (5.7)$$

Here we already assumed an evaporation process with an initial rate: $\dot{E}_0 = -|\dot{E}_0| < 0$. The thermodynamic length of the fluctuation, from E_0 at $t = 0$ to E_τ at $t = \tau$, is given by:

$$\mathcal{L}_{E_0 \rightarrow E_\tau} = \int_0^\tau \sqrt{g_{ab} \dot{x}^a \dot{x}^b} dt = \sqrt{-\epsilon} \frac{|\dot{E}_0| \sqrt[4]{\lambda}}{2^{3/4} E_0^{3/4} \sqrt{\zeta}} \tau = v\tau, \quad (5.8)$$

where $x^a(t) = (E(t), J(t) = 0)$, and v is the thermodynamic speed of the process. The length is real and positive if $\epsilon < 0$. On the other hand, directly computing the thermodynamic length by inserting $x^a = (E, J = 0)$, one finds:

$$\mathcal{L}_{E_0 \rightarrow E_\tau} = \int \sqrt{g_{ab} dx^a dx^b} = 2\sqrt[4]{2\lambda} \sqrt{\frac{-\epsilon}{\zeta}} \left(\sqrt[4]{E_0} - \sqrt[4]{E_\tau} \right). \quad (5.9)$$

Comparing both lengths we can estimate the average relaxation time $\bar{\tau}$ of the process:

$$\bar{\tau} \approx \frac{4E_0^{3/4}}{|\dot{E}_0|} \left(\sqrt[4]{E_0} - \sqrt[4]{E_\tau} \right). \quad (5.10)$$

The result for the average relaxation time is non-trivial. In the previous representation it was proportional to the entropy difference between the initial and the final state (4.11), here it involves the difference of the fourth root of the initial and the final energy of the BTZ black hole.

For a full optimal evaporation the time is $t_{evap} = 4E_0/|\dot{E}_0|$. Thus, the evaporation length is:

$$\mathcal{L}_{evap} = \frac{2\sqrt[4]{2\lambda}\sqrt{-\epsilon}}{\sqrt{\zeta}} \sqrt[4]{E_0} = 2\sqrt{\frac{-\epsilon\pi ck\ell}{\hbar}} \sqrt[4]{\frac{2E_0}{G_3}}. \quad (5.11)$$

The square of the thermodynamic length, \mathcal{L}^2 , carries units of entropy (Joules per Kelvin), consistent with its interpretation as the minimal entropy produced during the process. This interpretation allows one to determine the metric scale factor ϵ for the complete evaporation of the BTZ. In this case, it is reasonable to require that \mathcal{L}^2 be at least equal to the initial entropy of the BTZ black hole, given by $S_0 = \sqrt{2\lambda E_0}/\zeta$. Imposing this condition yields $\epsilon = -1/4$.

5.3 Optimal processes of the rotating BTZ black hole

In contrast to the results obtained in the energy representation, the entropy ensemble admits a broader variety of final configurations. For example, the analysis shows that certain optimal trajectories asymptotically guide the system toward near-extremal BTZ states. Yet this limit cannot be reached within finite classical time, in agreement with the third law of thermodynamics. Other trajectories instead drive the BTZ black hole toward a fixed, non-vanishing specific spin (far enough from extremality), while a third class of geodesics inevitably terminates in a static configuration within finite time.

5.3.1 Initial conditions

The initial state will be defined by the following initial parameters of the BTZ black hole:

$$E_0 = 5, \quad J_0 = 1, \quad S_0 = \pi\sqrt{\ell \left(E_0\ell + \sqrt{E_0^2\ell^2 - J_0^2} \right)} = 10, \quad a_0 = \frac{J_0}{E_0\ell} = 0.2, \quad (5.12)$$

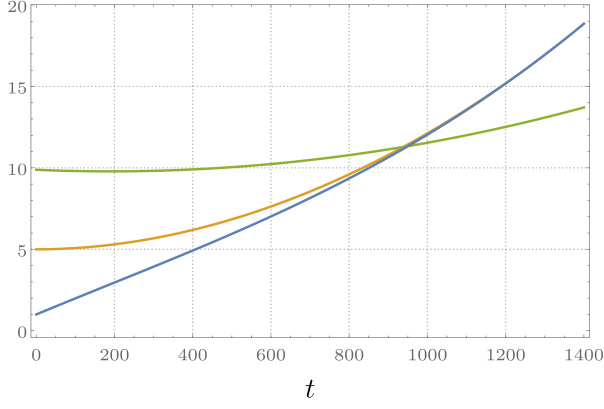
where $\ell = 1$. The initial rates of change will be presented in polar coordinates (u, ϕ) by:

$$\dot{E}_0 = u \sin \phi, \quad \dot{J}_0 = u \cos \phi, \quad u = \sqrt{\dot{E}_0^2 + \dot{J}_0^2}, \quad \tan \phi = \frac{\dot{E}_0}{\dot{J}_0}. \quad (5.13)$$

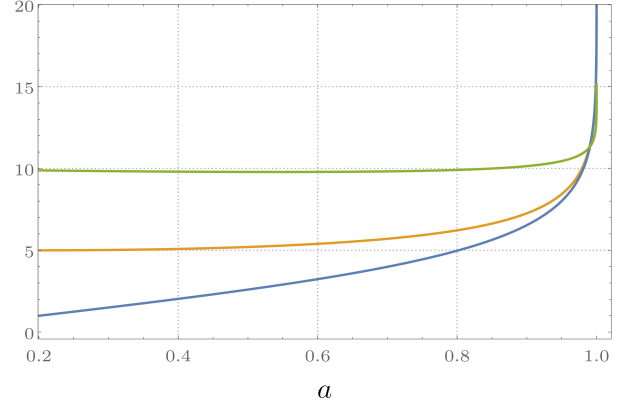
The initial rates for several angles ϕ and $u = 0.01$ are presented in Table 2. Their corresponding geodesic paths in (E, J) space are displayed on Figure 7. In this case, the thermodynamic curvature R is zero, thus the (E, J) space is Ricci flat.

5.3.2 Profiles at $\phi = 0^\circ$

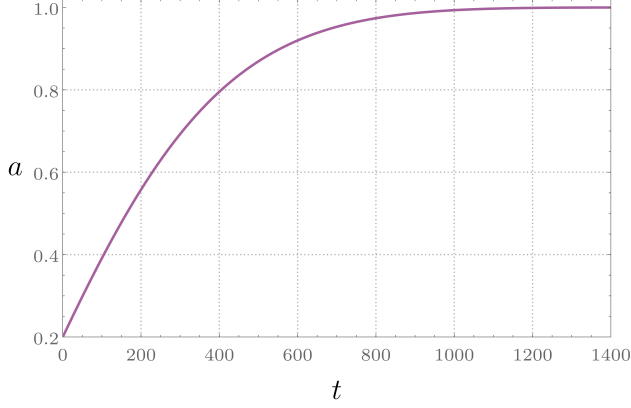
In this case, the specific spin $a(t)$ of the BTZ black hole asymptotically approaches its extremal value (Fig. 5c). Since this limit cannot be reached within finite time, the system continues to fluctuate indefinitely between nearly extremal states. The process leads to a monotonic growth of all black hole parameters, characterizing it as an accretion-type evolution.



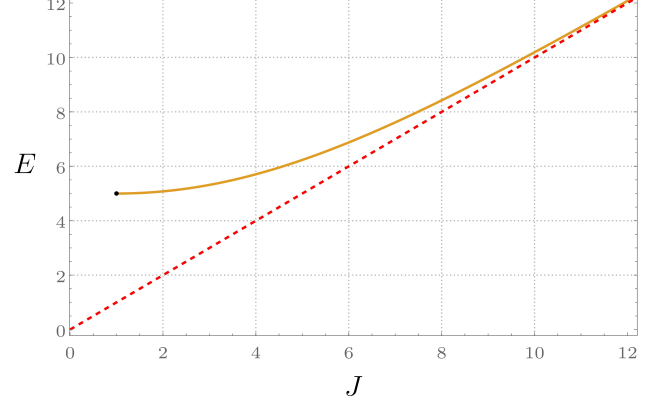
(a) Profiles $E(t)$, $S(t)$ and $J(t)$.



(b) Profiles $E(a)$, $S(a)$ and $J(a)$.



(c) The specific spin $a(t)$.

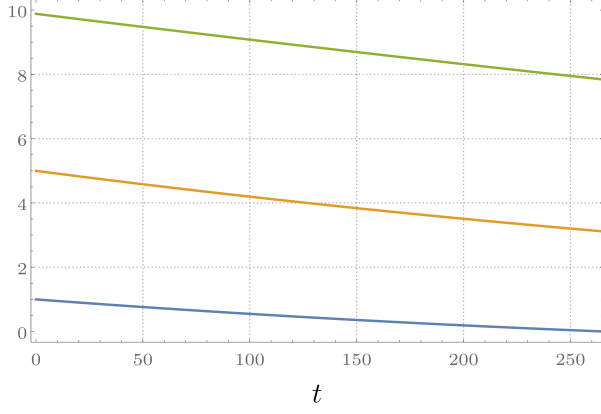


(d) The geodesic path of states in (E, J) space.

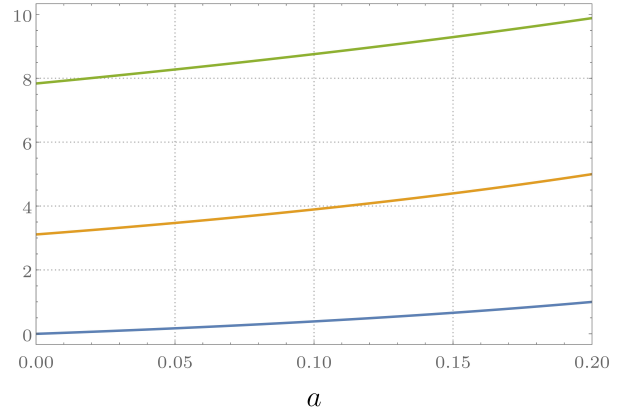
Figure 5: Profiles for $\phi = 0^\circ$. (a) Time evolution of E (orange), S (green), and J (blue). (b) The dependence of E , S , and J on the specific spin a . The BTZ black hole does not settle to a final state. It fluctuates between near-extremal states forever asymptotically approaching extremality. (c) Time evolution of the specific spin $a(t)$. The spin asymptotically increases towards the extremal value. (d) The geodesic trajectory of states (orange curve) in the (E, J) space starts at $E_0 = 5$ and $J_0 = 1$ (black dot), and asymptotically approaches the extremal curve (dashed red) over time.

5.3.3 Profiles at $\phi = 240^\circ$

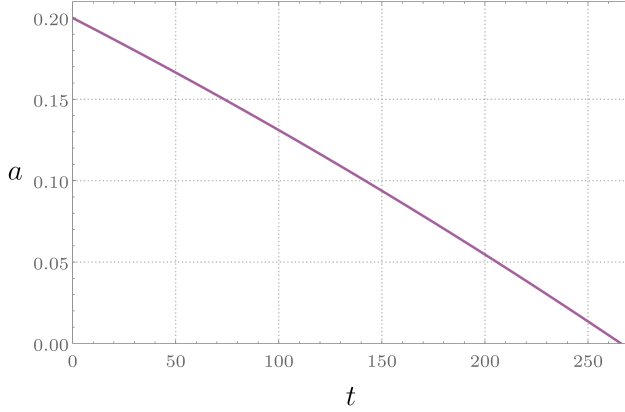
In this case, the specific spin $a(t)$ of the BTZ black hole decreases monotonically until it vanishes (Fig. 6c). All black hole parameters decrease during the evolution, indicating an evaporation-type process in which the BTZ black hole loses energy. The final state is a static configuration with energy $E_\tau = 0.6 E_0$ and entropy $S_\tau = 0.8 S_0$, corresponding to a reduction of about 40% in energy and 20% in entropy.



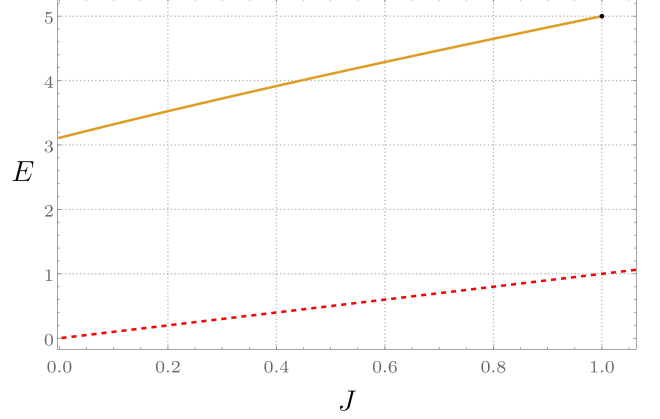
(a) Profiles $E(t)$, $S(t)$ and $J(t)$.



(b) Profiles $E(a)$, $S(a)$ and $J(a)$.



(c) The specific spin $a(t)$.



(d) The geodesic path of states in (E, J) space.

Figure 6: Profiles for $\phi = 240^\circ$. (a) Time evolution of E (orange), S (green), and J (blue). (b) The dependence of E , S , and J on the specific spin a . The BTZ black hole settles to a final static state with energy $E_\tau = 3$ and $S_\tau = 8$ in Planck units. (c) Time evolution of the specific spin $a(t)$. The spin monotonically decreases to zero. (d) The geodesic trajectory of states (orange curve) in the (E, J) space starts at $E_0 = 5$ and $J_0 = 1$ (black dot), and terminates when the angular momentum vanishes.

5.3.4 Summary for additional processes

Figure 7 displays representative geodesic trajectories in the (E, J) space, with the corresponding initial conditions summarized in Table 2. For initial angles ϕ in the range $0^\circ \leq \phi \leq 180^\circ$, the dynamics is predominantly governed by accretion-type optimal processes. As ϕ increases beyond 180° , evaporation channels become progressively more relevant. Complete evaporation of the BTZ black hole, however, is attained only asymptotically, requiring infinite time, and occurs exclusively for $\phi > 240^\circ$.

The late-time behavior of the system separates into distinct regimes determined by the angle ϕ . For $0^\circ \leq \phi \leq 45^\circ$, the evolution drives the system toward near-extremal configurations with $a_\tau \rightarrow 1$. In the range $45^\circ < \phi \leq 90^\circ$, the trajectories instead approach non-extremal states with spin parameter $a < 1$. For intermediate angles, $90^\circ < \phi \leq 240^\circ$, the dynamics settle into static final configurations within finite time. Beyond this window, at large angles $\phi > 240^\circ$, the system is driven asymptotically toward extremality, but via evaporation.

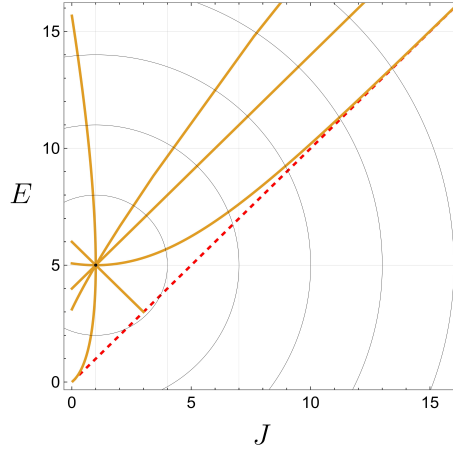


Figure 7: Geodesic trajectories of states in the (E, J) space. Since the thermodynamic curvature is $R = 0$, the manifold is Ricci-flat. The initial state $(E_0 = 5, J_0 = 1)$ is far from the extremal boundary (dashed red curve). The figure presents a magnified view around this initial point. Concentric polar circles indicate the initial angles ϕ , which set the direction of the corresponding geodesics. Each trajectory evolves toward a distinct final configuration, corresponding either to a near-extremal ($a_\tau \rightarrow 1$), finite spinning state ($0 < a_\tau < 1$), or a static BTZ black hole $a_\tau = 0$.

ϕ	$\dot{E}_0 10^{-3}$	$\dot{S}_0 10^{-3}$	$\dot{J}_0 10^{-3}$	$\dot{a}_0 10^{-3}$	a_τ	E_τ	$\delta E \%$	S_τ	$\delta S \%$	τ	\mathcal{L}^2
0°	0.0	-1.0	10	2.0	$\rightarrow 1$	$\rightarrow \infty$	-	$\rightarrow \infty$	-	$\rightarrow \infty$	$\rightarrow \infty$
45°	7.1	6.4	7.1	1.1	$\rightarrow 1$	$\rightarrow \infty$	-	$\rightarrow \infty$	-	$\rightarrow \infty$	$\rightarrow \infty$
60°	8.7	8.2	5.0	0.7	$\rightarrow 0.966$	$\rightarrow \infty$	-	$\rightarrow \infty$	-	$\rightarrow \infty$	$\rightarrow \infty$
70°	9.4	9.1	3.4	3.1	$\rightarrow 0.725$	$\rightarrow \infty$	-	$\rightarrow \infty$	-	$\rightarrow \infty$	$\rightarrow \infty$
90°	10	10	0.0	-0.4	0.0	16	+213	18	+78	651	4.5
135°	7.1	7.9	-7.1	-1.7	0.0	6.0	+20	11	+10	121	0.2
180°	0.0	1.0	-10	-2.0	0.0	5.1	+2	10	+0	98	0.1
225°	-7.1	-6.4	-7.1	-1.1	0.0	4.0	-20	9.0	-10	164	0.2
240°	-8.7	-8.2	-5.0	-0.7	0.0	3.0	-38	8.0	-20	266	0.6
270°	-10	-10	0.0	0.4	$\rightarrow 1$	$\rightarrow 0$	-	$\rightarrow 0$	-	$\rightarrow \infty$	$\rightarrow \infty$
315°	-7.1	-7.9	7.1	1.7	$\rightarrow 1$	$\rightarrow 0$	-	$\rightarrow 0$	-	$\rightarrow \infty$	$\rightarrow \infty$

Table 2: The table summarizes the initial rates of key parameters across various processes. It also indicates how the final state differs from the initial BTZ configuration after each process. Additionally, the duration τ of the process (in Planck units) and the thermodynamic length squared, \mathcal{L}^2 , are provided. The quantity \mathcal{L}^2 is the minimal entropy produced during the transformation. Smaller \mathcal{L} indicates higher probability for the process to occur.

6 Conclusion

In this work, we investigated the finite-time optimal thermodynamics of the BTZ black hole in both the energy and entropy ensembles using the thermogeometric optimization framework developed in [31].

By applying the differential Sylvester criterion (2.11), we demonstrated that the BTZ black hole is thermodynamically stable. This conclusion is further supported by the positive-definite behavior of the relevant local heat capacities (2.14)–(2.12). These results also indicate the absence of Davies-type phase transitions in the BTZ state space, aside from the extremal limit.

In the energy representation, we employed the Weinhold thermodynamic metric (4.1), which possesses a nonvanishing thermodynamic curvature (4.2). Within this framework, we showed that the curvature (R) remains positive (Fig. 1), signifying that the corresponding information geometry is intrinsically elliptic. This geometric feature is reflected also by the positive definiteness of the thermodynamic length for all optimal processes considered.

For the static BTZ black hole, we obtained analytic expressions for both the thermodynamic length (4.10) and the relaxation time (4.11) associated with the optimal evaporation process. Both quantities were found to scale proportionally with the entropy change $\Delta S = S_0 - S_\tau$ generated along the trajectory. Consequently, larger black holes exhibit lower process probabilities and correspondingly longer evaporation times.

For the rotating BTZ black hole, we performed a numerical analysis of the optimal processes induced by parameter variations. In all cases examined within the energy representation, the system evolves toward a static (non-rotating) configuration with well-defined energy and entropy, preventing complete evaporation. Additionally, we observed that at most two optimal geodesics can connect any pair of admissible macrostates (see Fig. 4), a feature permitted only in spaces of positive curvature. A summary of results for a range of initial conditions is given in Table 1.

Contrary to the situation observed in the energy representation, the entropy ensemble for the rotating BTZ black hole allows a richer set of final states, even though its information metric is flat. Our analysis shows that certain optimal trajectories asymptotically drive the system toward near-extremal configurations, consistent with the third law of thermodynamics, which forbids reaching extremality in finite classical time. Other trajectories approach a fixed, nonvanishing specific spin away from extremality, while a third class terminates in a static configuration within finite time. These results are summarized in Table 2.

For the static BTZ black hole in the entropy representation, the evaporation thermodynamic length (5.9) and consequently the relaxation time (5.10) scale with the fourth root of the black hole energy suggesting once again that larger black holes evaporate more slowly.

All analyses were carried out in SI units, enabling a consistent interpretation of the thermodynamic length either as the minimal energy required for a given process or as the minimal entropy produced along an optimal trajectory. This facilitated the determination of the probability strength factor (the metric scale) ϵ governing evaporation. In the energy representation we obtained $\epsilon = 1/2$, whereas in the entropy representation we found $\epsilon = -1/4$. In both cases, these values ensure a physically meaningful probability and guarantee that thermodynamic length remains positive-definite along geodesic paths.

Finally, it would be interesting to extend this optimization analysis to more general or fundamentally distinct black hole solutions in (2+1) dimensions, including warped black holes [44, 45], Lifshitz solutions [46–48], regular black holes [49–51], noncommutative geometries [52, 53], Chern–Simons black holes [54–56], Gauss–Bonnet-like theories [57], and other modified-gravity or exotic solutions [58–61].

Acknowledgments

We are very grateful to H. Dimov, S. Yazadjiev, D. Marvakov and P. Ivanov for their useful comments and discussions. G. S. thankfully acknowledges the support by the Sofia University grant 80-10-52/2025. M. R. was fully supported by Bulgarian NSF grant KP-06-H88/3. R. R. and T. V. were fully financed by the European Union- NextGeneration EU, through the National Recovery and Resilience Plan of the Republic of Bulgaria, project BG-RRP-2.004-0008-C01. The authors express their sincere gratitude to CERN, SEENET-MTP, ICTP, EPS, the Simons Foundation, and the International Center for Mathematical Sciences (ICMS) in Sofia for their support in funding and organizing various annual scientific events.

A Planck parameters in (2+1)-dimensions related to G_3

In Planck units $\hbar = c = G_3 = k = 1$ everything is dimensionless and can be expressed as how many times a given quantity enters in its corresponding SI unit quantity. For example if L is dimensionless length then its SI version is restored by $L_{(\text{SI})} = LL_{\text{P}}^{(3)}$, where $L_{\text{P}}^{(3)}$ is the (2+1)-dimensional Planck length related to G_3 . In this case, the replacement rule is actually $L \rightarrow L_{(\text{SI})}/L_{\text{P}}^{(3)}$. The (2+1)-dimensional Planck system of units related to G_3 can be extracted by a simple dimensionless analysis from:

$$P = \hbar^x G_3^y c^z k^u = [M^{u+x-y} L^{2u+2(x+y)+z} T^{-2u-x-2y-z} K^{-u}]. \quad (\text{A.1})$$

The relevant (2+1)-dimensional Planck units are given by:

$$L_{\text{P}}^{(3)} = \frac{\hbar G_3}{c^3}, \quad M_{\text{P}}^{(3)} = \frac{c^2}{G_3}, \quad E_{\text{P}}^{(3)} = \frac{c^4}{G_3}, \quad t_{\text{P}}^{(3)} = \frac{\hbar G_3}{c^4}, \quad T_{\text{P}}^{(3)} = \frac{c^4}{G_3 k}, \quad S_{\text{P}}^{(3)} = k, \quad J_{\text{P}}^{(3)} = \hbar, \quad (\text{A.2})$$

where $L_{\text{P}}^{(3)}$ is length, $M_{\text{P}}^{(3)}$ is mass, $E_{\text{P}}^{(3)}$ is energy, $t_{\text{P}}^{(3)}$ is time, $T_{\text{P}}^{(3)}$ is temperature, $S_{\text{P}}^{(3)}$ is entropy, and $J_{\text{P}}^{(3)}$ is angular momentum. The BTZ thermodynamics in Planck units is defined by:

$$\lambda \rightarrow \pi^2, \quad \zeta \rightarrow \frac{1}{\ell}, \quad (\text{A.3})$$

where the AdS radius ℓ is now a dimensionless parameter. As an example, let us restore the SI units of the evaporation thermodynamic length from (4.13). In Planck units it is given by:

$$\mathcal{L} = \frac{S_0}{\pi \ell}, \quad (\text{A.4})$$

where \mathcal{L} , S_0 and ℓ are dimensionless. Since $\mathcal{L}_{(\text{SI})}^2$ represents an energy, its SI unit is Joule. Accordingly, $S_0^{(\text{SI})}$ has units of Joules/Kelvin, and $\ell_{(\text{SI})}$ has units of length. Thus, the following replacement rules restore the appropriate factors of the fundamental constants:

$$\mathcal{L}^2 \rightarrow \frac{\mathcal{L}_{(\text{SI})}^2}{E_{\text{P}}^{(3)}}, \quad S_0 \rightarrow \frac{S_0^{(\text{SI})}}{k}, \quad \ell \rightarrow \frac{\ell_{(\text{SI})}}{L_{\text{P}}^{(3)}}. \quad (\text{A.5})$$

At the end, one may skip the (SI) notation from the quantities.

B The BTZ solution in Planck and other units

Solving (2.2) for the horizon radii in terms of the energy and angular momentum, one obtains:

$$r_+ = \frac{2\ell}{c^2} \sqrt{\left(1 + \sqrt{1 - a^2}\right) G_3 E}, \quad r_- = \frac{2G_3 a E \ell}{c^2 \sqrt{\left(1 + \sqrt{1 - a^2}\right) G_3 E}}, \quad a = \frac{cJ}{E\ell}, \quad (\text{B.1})$$

where $a \in [0, 1)$ is the dimensionless specific spin parameter of the BTZ black hole. Using these expressions, the BTZ metric (2.1) can be written in the form:

$$ds^2 = \left(\frac{8G_3 E}{c^4} - \frac{r^2}{\ell^2} \right) c^2 dt^2 + \frac{dr^2}{\frac{r^2}{\ell^2} + \frac{16\ell^2 G_3^2 a^2 E^2}{c^8 r^2} - \frac{8G_3 E}{c^4}} - \frac{8aEG_3\ell}{c^3} dt d\varphi + r^2 d\varphi^2, \quad (\text{B.2})$$

In Planck units $c = G_3 = 1$ one has $E = M$ and:

$$ds^2 = \left(8M - \frac{r^2}{\ell^2} \right) dt^2 + \frac{dr^2}{\frac{J^2}{4r^2} + \frac{r^2}{\ell^2} - 8M} - 8J dt d\varphi + r^2 d\varphi^2. \quad (\text{B.3})$$

Note that by setting $c = 8G_3 = 1$ one recovers the original form of the BTZ metric [36, 40]:

$$ds^2 = \left(M - \frac{r^2}{\ell^2} \right) dt^2 + \frac{dr^2}{\frac{J^2}{4r^2} + \frac{r^2}{\ell^2} - M} - J dt d\varphi + r^2 d\varphi^2. \quad (\text{B.4})$$

References

- [1] J. P. Luminet, “Image of a spherical black hole with thin accretion disk,” *Astron. Astrophys.* **75** (1979) 228–235.
- [2] D. N. Page and K. S. Thorne, “Disk-Accretion onto a Black Hole. Time-Averaged Structure of Accretion Disk,” *Astrophys. J.* **191** (1974) 499–506.
- [3] K. S. Thorne, “Disk accretion onto a black hole. 2. Evolution of the hole,” *Astrophys. J.* **191** (1974) 507–520.
- [4] G. Gylchev, P. Nedkova, T. Vetsov, and S. Yazadjiev, “Image of the Janis-Newman-Winicour naked singularity with a thin accretion disk,” *Phys. Rev. D* **100** no. 2, (2019) 024055, [arXiv:1905.05273 \[gr-qc\]](#).
- [5] G. Gylchev, P. Nedkova, T. Vetsov, and S. Yazadjiev, “Image of the thin accretion disk around compact objects in the Einstein–Gauss–Bonnet gravity,” *Eur. Phys. J. C* **81** no. 10, (2021) 885, [arXiv:2106.14697 \[gr-qc\]](#).
- [6] **LIGO Scientific, Virgo** Collaboration, B. P. Abbott *et al.*, “Observation of Gravitational Waves from a Binary Black Hole Merger,” *Phys. Rev. Lett.* **116** no. 6, (2016) 061102, [arXiv:1602.03837 \[gr-qc\]](#).
- [7] L. Collaboration, B. P. Abbott, *et al.*, “Properties of the binary black hole merger gw150914,” *Phys. Rev. Lett.* **116** no. 24, (2016) 241102, [arXiv:1602.03840 \[gr-qc\]](#). <http://arxiv.org/abs/1602.03840>.
- [8] J. H. Taylor and J. M. Weisberg, “A new test of general relativity - gravitational radiation and the binary pulsar psr 1913+16,” *Astrophys. J.* **253** (Feb., 1982) 908–920. <http://dx.doi.org/10.1086/159690>.
- [9] S. W. Hawking, “Particle Creation by Black Holes,” *Commun. Math. Phys.* **43** (1975) 199–220. [Erratum: *Commun.Math.Phys.* 46, 206 (1976)].
- [10] R. Penrose and R. Floyd, “Extraction of rotational energy from a black hole,” *Nature Physical Science* **229** no. 6, (1971) 177–179. <http://dx.doi.org/10.1038/physci229177a0>.
- [11] F. Weinhold, “Metric geometry of equilibrium thermodynamics,” *J. Chem. Phys.* **63** no. 6, (1975) 2479–2483. <http://dx.doi.org/10.1063/1.431689>.
- [12] G. Ruppeiner, “Thermodynamic Critical Fluctuation Theory?,” *Phys. Rev. Lett.* **50** (1983) 287–290.
- [13] G. Ruppeiner, “Riemannian geometry in thermodynamic fluctuation theory,” *Rev. Mod. Phys.* **67** (1995) 605–659. <http://dx.doi.org/10.1103/RevModPhys.67.605>.
- [14] P. Salamon, J. Nulton, and E. Ihrig, “On the relation between entropy and energy versions of thermodynamic length,” *J. Chem. Phys.* **80** no. 1, (Jan., 1984) 436–437. <http://dx.doi.org/10.1063/1.446468>.
- [15] R. Mrugala, “On equivalence of two metrics in classical thermodynamics,” *Physica A: Statistical Mechanics and its Applications* **125** no. 2–3, (1984) 631–639. [http://dx.doi.org/10.1016/0378-4371\(84\)90064-1](http://dx.doi.org/10.1016/0378-4371(84)90064-1).

- [16] H. Quevedo and A. Vazquez, “The Geometry of thermodynamics,” *AIP Conf. Proc.* **977** no. 1, (2008) 165–172, [arXiv:0712.0868 \[math-ph\]](#).
- [17] H. Quevedo, “Geometrothermodynamics of black holes,” *Gen. Rel. Grav.* **40** (2008) 971–984, [arXiv:0704.3102 \[gr-qc\]](#).
- [18] H. Quevedo, M. N. Quevedo, and A. Sanchez, “Homogeneity and thermodynamic identities in geometrothermodynamics,” *Eur. Phys. J. C* **77** no. 3, (2017) 158, [arXiv:1701.06702 \[gr-qc\]](#).
- [19] V. Pineda, H. Quevedo, M. N. Quevedo, A. Sanchez, and E. Valdes, “The physical significance of geometrothermodynamic metrics,” *Int. J. Geom. Methods Mod. Phys.* **16** no. 11, (2019) 1950168.
- [20] H. Quevedo and M. N. Quevedo, “Unified representation of homogeneous and quasi-homogenous systems in geometrothermodynamics,” *Phys. Lett. B* **838** (2023) 137678.
- [21] G. Ruppeiner, “Stability and fluctuations in black hole thermodynamics,” *Phys. Rev. D* **75** (2007) 024037.
- [22] S. A. H. Mansoori, B. Mirza, and E. Sharifian, “Extrinsic and intrinsic curvatures in thermodynamic geometry,” *Phys. Lett. B* **759** (2016) 298–305, [arXiv:1602.03066 \[gr-qc\]](#).
- [23] T. Vetsov, “Information Geometry on the Space of Equilibrium States of Black Holes in Higher Derivative Theories,” *Eur. Phys. J. C* **79** no. 1, (2019) 71, [arXiv:1806.05011 \[gr-qc\]](#).
- [24] F. A. M. Ramírez, *Quantum critical effects in the spectrum of excited states*. PhD thesis, Univerzita Karlova, Matematicko-fyzikální fakulta, Praha, 2025. <https://dspace.cuni.cz/bitstream/handle/20.500.11956/200761/140132116.pdf?sequence=1&isAllowed=y>. PhD thesis.
- [25] B. Andresen, “Finite-time thermodynamics and thermodynamic length,” *Revue Générale de Thermique* **35** no. 418–419, (1996) 621–650.
- [26] G. E. Crooks, “Measuring thermodynamic length,” *Phys. Rev. Lett.* **99** no. 10, (2007) 100602, [arXiv:0706.0559 \[cond-mat.stat-mech\]](#).
- [27] C. Cafaro, O. Luongo, S. Mancini, and H. Quevedo, “Thermodynamic length, geometric efficiency and legendre invariance,” *Physica A* **590** (2022) 126740.
- [28] P. Salamon, B. Andresen, and R. S. Berry, “Thermodynamics in finite time. II. Potentials for finite-time processes,” *Phys. Rev. A* **15** no. 5, (1977) 2094–2102.
- [29] B. Andresen, P. Salamon, and R. S. Berry, “Thermodynamics in finite time. Extremals for imperfect heat engines,” *J. Chem. Phys.* **66** no. 4, (1977) 1571–1577.
- [30] P. Salamon, J. D. Nulton, and R. S. Berry, “Length in Statistical Thermodynamics,” *J. Chem. Phys.* **82** no. 1, (1985) 2433–2436.
- [31] V. Avramov, H. Dimov, M. Radomirov, R. C. Rashkov, and T. Vetsov, “Black holes and thermogeometric optimization,” *Eur. Phys. J. C* **85** no. 5, (2025) 587, [arXiv:2410.11128 \[gr-qc\]](#).

- [32] A. Bravetti, C. Gruber, and C. S. Lopez-Monsalvo, “Thermodynamic optimization of a Penrose process: An engineers’ approach to black hole thermodynamics,” *Phys. Rev. D* **93** no. 6, (2016) 064070, [arXiv:1511.06801 \[gr-qc\]](#).
- [33] C. Gruber, O. Luongo, and H. Quevedo, “Geometric approaches to the thermodynamics of black holes,” in *14th Marcel Grossmann Meeting on Recent Developments in Theoretical and Experimental General Relativity, Astrophysics, and Relativistic Field Theories*, vol. 1, pp. 453–466. 2017. [arXiv:1603.09443 \[gr-qc\]](#).
- [34] V. Avramov, H. Dimov, M. Radomirov, R. C. Rashkov, and T. Vetsov, “Thermodynamic stability of acgl chern-simons black hole and optimal processes,” *Annals of the University of Craiova, Physics* **33** (2023) 78–97.
- [35] V. Avramov, H. Dimov, M. Radomirov, R. C. Rashkov, and T. Vetsov, “Thermodynamic Length and Optimal Processes in Holographic Models,” in *15th International Workshop on Lie Theory and Its Applications in Physics*. 2025.
- [36] M. Banados, C. Teitelboim, and J. Zanelli, “The Black hole in three-dimensional space-time,” *Phys. Rev. Lett.* **69** (1992) 1849–1851, [arXiv:hep-th/9204099](#).
- [37] J. M. Maldacena, “The large n limit of superconformal field theories and supergravity,” *Adv. Theor. Math. Phys.* **2** (1998) 231–252, [hep-th/9711200](#).
- [38] A. Strominger, “Black hole entropy from near-horizon microstates,” *JHEP* **02** (1998) 009, [hep-th/9712251](#).
- [39] J. D. Brown and M. Henneaux, “Central charges in the canonical realization of asymptotic symmetries: An example from three-dimensional gravity,” *Commun. Math. Phys.* **104** (1986) 207–226.
- [40] S. Carlip, “The (2+1)-Dimensional black hole,” *Class. Quant. Grav.* **12** (1995) 2853–2880, [arXiv:gr-qc/9506079](#).
- [41] S. Carlip, “Conformal field theory, (2+1)-dimensional gravity, and the BTZ black hole,” *Class. Quant. Grav.* **22** (2005) R85–R124, [arXiv:gr-qc/0503022](#).
- [42] V. Avramov, H. Dimov, M. Radomirov, R. C. Rashkov, and T. Vetsov, “On thermodynamic stability of black holes. Part I: classical stability,” *Eur. Phys. J. C* **84** no. 3, (2024) 281, [arXiv:2302.11998 \[gr-qc\]](#).
- [43] V. Avramov, H. Dimov, M. Radomirov, R. C. Rashkov, and T. Vetsov, “On thermodynamic stability of black holes. part ii: Ads family of solutions,” 2024.
- [44] D. Anninos, W. Li, M. Padi, W. Song, and A. Strominger, “Warped AdS(3) Black Holes,” *JHEP* **03** (2009) 130, [arXiv:0807.3040 \[hep-th\]](#).
- [45] E. Tonni, “Warped black holes in 3D general massive gravity,” *JHEP* **08** (2010) 070, [arXiv:1006.3489 \[hep-th\]](#).
- [46] E. Ayon-Beato, A. Garbarz, G. Giribet, and M. Hassaine, “Lifshitz Black Hole in Three Dimensions,” *Phys. Rev. D* **80** (2009) 104029, [arXiv:0909.1347 \[hep-th\]](#).
- [47] Ö. Sarıoğlu, “Stationary Lifshitz Black Hole of New Massive Gravity,” *Class. Quant. Grav.* **36** no. 1, (2019) 015015, [arXiv:1806.10811 \[gr-qc\]](#).

- [48] A. Herrera-Aguilar, J. A. Herrera-Mendoza, and D. F. Higuera-Borja, “Rotating spacetimes generalizing Lifshitz black holes,” *Eur. Phys. J. C* **81** no. 10, (2021) 874, [arXiv:2104.14514 \[hep-th\]](#).
- [49] P. Bueno, P. A. Cano, J. Moreno, and G. van der Velde, “Regular black holes in three dimensions,” *Phys. Rev. D* **104** no. 2, (2021) L021501, [arXiv:2104.10172 \[gr-qc\]](#).
- [50] T. Karakasis, E. Papantonopoulos, Z.-Y. Tang, and B. Wang, “(2+1)-dimensional black holes in $f(R, \phi)$ gravity,” *Phys. Rev. D* **105** no. 4, (2022) 044038, [arXiv:2201.00035 \[gr-qc\]](#).
- [51] S. N. Sajadi, M. Khodadi, O. Luongo, and H. Quevedo, “Anisotropic generalized polytropic spheres: Regular 3D black holes,” *Phys. Dark Univ.* **45** (2024) 101525, [arXiv:2312.16081 \[gr-qc\]](#).
- [52] F. Rahaman, P. K. F. Kuhfittig, B. C. Bhui, M. Rahaman, S. Ray, and U. F. Mondal, “BTZ black holes inspired by noncommutative geometry,” *Phys. Rev. D* **87** no. 8, (2013) 084014, [arXiv:1301.4217 \[gr-qc\]](#).
- [53] B. Hamil and B. C. Lütfüoğlu, “Thermodynamics and Heat Engine Behavior of Phantom BTZ Black Holes in Noncommutative Geometry,” [arXiv:2503.03725 \[hep-th\]](#).
- [54] K. A. Moussa and G. Clement, “Topologically massive gravitoelectrodynamics: Exact solutions,” *Class. Quant. Grav.* **13** (1996) 2319–2328, [arXiv:gr-qc/9602034](#).
- [55] K. A. Moussa, G. Clement, H. Guennoune, and C. Leygnac, “Three-dimensional Chern-Simons black holes,” *Phys. Rev. D* **78** (2008) 064065, [arXiv:0807.4241 \[gr-qc\]](#).
- [56] K. A. Moussa, G. Clément, and H. Guennoune, “Chern–Simons dilaton black holes in $2 + 1$ dimensions,” *Class. Quant. Grav.* **33** no. 6, (2016) 065008, [arXiv:1510.07152 \[gr-qc\]](#).
- [57] R. A. Hennigar, D. Kubiznak, and R. B. Mann, “Rotating Gauss-Bonnet BTZ Black Holes,” *Class. Quant. Grav.* **38** no. 3, (2021) 03LT01, [arXiv:2005.13732 \[gr-qc\]](#).
- [58] M. Papajčák, *Exact spacetimes in 2+1 gravity*. PhD thesis, Charles U., 2022.
- [59] T. Karakasis, E. Papantonopoulos, Z.-Y. Tang, and B. Wang, “Rotating (2+1)-dimensional black holes in Einstein-Maxwell-dilaton theory,” *Phys. Rev. D* **107** no. 2, (2023) 024043, [arXiv:2210.15704 \[gr-qc\]](#).
- [60] T. Karakasis, G. Koutsoumbas, and E. Papantonopoulos, “Black holes with scalar hair in three dimensions,” *Phys. Rev. D* **107** no. 12, (2023) 124047, [arXiv:2305.00686 \[gr-qc\]](#).
- [61] K. Jusufi, M. Jamil, and A. Sheykhi, “Three-dimensional charged black holes in Gauss–Bonnet gravity,” *Eur. Phys. J. C* **83** no. 11, (2023) 1039, [arXiv:2302.10799 \[physics.gen-ph\]](#).